Journal of Polymers and the Environment (2022) 30:1344–1354
https://doi.org/10.1007/s10924-021-02278-0

ORIGINAL PAPER

Diethylenetriaminepentaacetic Acid (DPTA)-modified Magnetic Cellulose Nanocrystals can Efficiently Remove Pb(II) from Aqueous Solution

Jian Shen[1] · Fangyuan Jiang[2] · Nan Wang[2] · Xiao–kun Ouyang[2] · Mi-cong Jin[3]

Accepted: 26 August 2021 / Published online: 2 September 2021

Abstract

Surface modification of cellulose nanocrystals (CNC) is essential for improving their reactivity and adsorption capacity. Oxidation, as a conventional modification method of CNC, has strong reaction conditions, which may partially destroy the structure of CNCs. Herein, we propose a mild cellulose modification method, in which diethylenetriaminepentaacetic acid (DPTA) was grafted onto CNC with an aminosilane coupling agent. To facilitate the enrichment and recovery of adsorbents, we prepared magnetic CNC before grafting DPTA, and finally obtained magnetic carboxylic functionalized CNC (MCNC-DPTA). The effects of the reaction parameters on the adsorption process were systematically studied by transmission electron microscopy, X-ray diffraction, Vibration sample magnetometry, Fourier transform infrared spectroscopy, and X-ray photoelectron spectroscopy. Additionally, the effects of the solution pH, the initial concentration of Pb, and the adsorption time on the adsorption properties of the materials were evaluated. Furthermore, the structure, morphology, and thermal properties of the solution were systematically studied. After 6 cycle tests, the adsorption amount of Pb(II) by MCNC-DPTA was only reduced by 7%. These results show that MCNC-DPTA is an environment-friendly adsorption material with an excellent Pb(II) removal effect.

Keywords Cellulose nanocrystals · Carboxylation · Adsorbent · Pb(II)

Introduction

It is difficult for heavy metals to degrade under natural conditions, and with the passage of time, the quantities of heavy metals tend to show a positive growth trend [1, 2]. For example, lead is widely used in construction, lead-acid batteries, warheads, and welding materials; the improper disposal treatment of such materials can lead to the release of Pb(II) into the environment[3], ultimately leading to the accumulation of Pb(II) in the human body [4, 5]. Lead poisoning is caused if the cumulative level of Pb(II) in the blood of a human adults is > 0.1 mg/L, which is highly detrimental to human health and may even cause death. Adsorption is a commonly used method for the treatment of water to remove such heavy metal ions [6–8]; thus, the development of adsorbents exhibiting good stability, excellent performance, low cost, and facile regeneration continues to be a significant research focus [8–10].

Biomass adsorbents are considered ideal materials for heavy metal removal because they do not lead to secondary pollution [11–13]. Among them, cellulose is the most

✉ Jian Shen
nbutjianshen@163.com

✉ Xiao–kun Ouyang
xkouyang@zjou.edu.cn

✉ Mi-cong Jin
jmcjc@163.com

[1] School of Materials and Chemical Engineering, Ningbo University of Technology, Ningbo 315211, People's Republic of China

[2] School of Food and Pharmacy, Zhejiang Ocean University, Haida Nan Load 1#, Lincheng, Zhoushan 316022, People's Republic of China

[3] Key Laboratory of Health Risk Appraisal for Trace Toxic Chemicals of Zhejiang Province, Ningbo Municipal Center for Disease Control and Prevention, Ningbo, Zhejiang 315010, People's Republic of China

widely distributed and abundant biomass material in nature [14]. Importantly, cellulose is non-toxic, costs less, can be easily sourced, and exhibits good chemical stability and biodegradability [15–18]. Cellulose nanocrystals (CNC), a type of cellulose, are a suitable adsorbent because they have sizes on the order of several nanometers and possess a large specific surface area and high mechanical strength [19, 20]. In terms of its molecular structure, cellulose is a linear natural polymer composed of glucoside repeating units that are linked by β-1,4 glycosidic bonds. Numerous intramolecular and intermolecular hydrogen bonds are formed between cellulose chains, greatly reducing the adsorption efficiency of cellulose. Thus, the adsorption efficiency of cellulose must be improved through a range of modification approaches.

Anionic functional groups, such as carboxyl and sulfonic acid residues [21, 22], show high affinity toward heavy metal ions because of the electrostatic attraction between the functional groups and ions. For example, ethylenediaminetetraacetic acid (EDTA) and diethylenetriaminepentaacetic acid (DPTA) are commonly used compounds, and an EDTA-modified magnetic chitosan composite has been applied to remove both anionic dyes and heavy metals [23, 24]. Similarly, DPTA has been used to modify microcrystalline cellulose and serves as an effective Hg(II) adsorbent [25].

However, CNC contain only hydroxyl groups, which restricts their adsorption properties toward heavy metal ions. Therefore, modification to form carboxyl moieties is desirable to improve the adsorption capacities of CNC toward heavy metals. In this context, a conventional approach for cellulose modification is the oxidation of the hydroxyl groups to more reactive aldehydes and ketones through the use of strong oxidants. For example, CNC have been oxidized using periodates to introduce dialdehyde groups, which can participate in crosslinking [26]; Cellulose in bleached pulp was oxidized by sodium periodate and TEMPO-NaClO/NaBr to obtain carboxylated cellulose [27]. However, the use of strong oxidants can have a detrimental effect on the structure of cellulose, and common oxidants such as ammonium ceric nitrate and sodium periodate pose a threat to both human health and the environment. The development of mild methods for cellulose modification is, therefore of particular interest.

Silane coupling agents (SCAs) are low-toxicity crosslinkers that can perform well under mild reaction conditions. SCAs have the common structure of Y-R–Si$(OR)_3$, where SiOR is a siloxy group and Y is an organic functional group. Importantly, the siloxy group can react with inorganic substances, whereas organic functional groups can react with organic compounds. As a result, SCAs such as (3-aminopropyl)triethoxysilane (APTES) and [3-(2,3-epoxypropoxy)propyl]trimethoxysilane (EPPTMS) have been used to modify inorganic nanoparticles such as magnetic and silica nanoparticles [28–30].

Thus, we prepared magnetic CNC (MCNC) and the use of SCAs to combine the MCNC with carboxyl-containing compounds. For this purpose, APTES is employed as the crosslinker to graft the siloxy group of the SCA onto the hydroxyl groups of the CNC and the magnetic nanoparticles; the amino moiety in the SCA binds to the carboxyl groups (DPTA) through amidation (Scheme 1). Using APTES as the crosslinker to graft DPTA, MCNC containing multiple carboxyl sites are prepared in a mild manner, and the behavior and mechanism of Pb(II) adsorption by MCNC-DPTA are investigated, the adsorption mechanism is shown in Fig. 1.

Materials and Methods

Materials

The CNCs were provided by Chemkey Advanced Materials (Shanghai, China). Chemical reagents used in the experiments are of analytical or spectroscopic grade and purchased from commercial suppliers. *N*-Hydroxy succinimide (NHS), 1-ethyl-3-(3-dimethylaminopropyl)carbodiimide (EDC), ferrous chloride tetrahydrate ($FeCl_2{\cdot}4H_2O$), ferric chloride hexahydrate ($FeCl_3{\cdot}6H_2O$), APTES, and DPTA

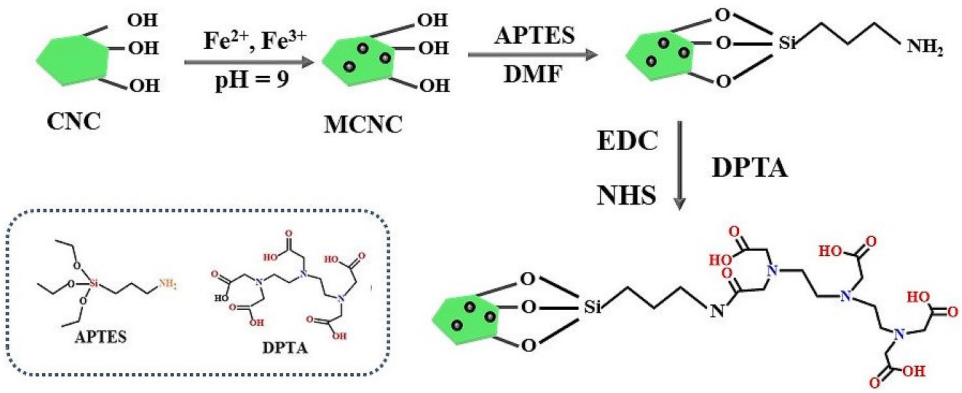

Scheme 1 Schematic representation of the preparation of MCNC-DPTA

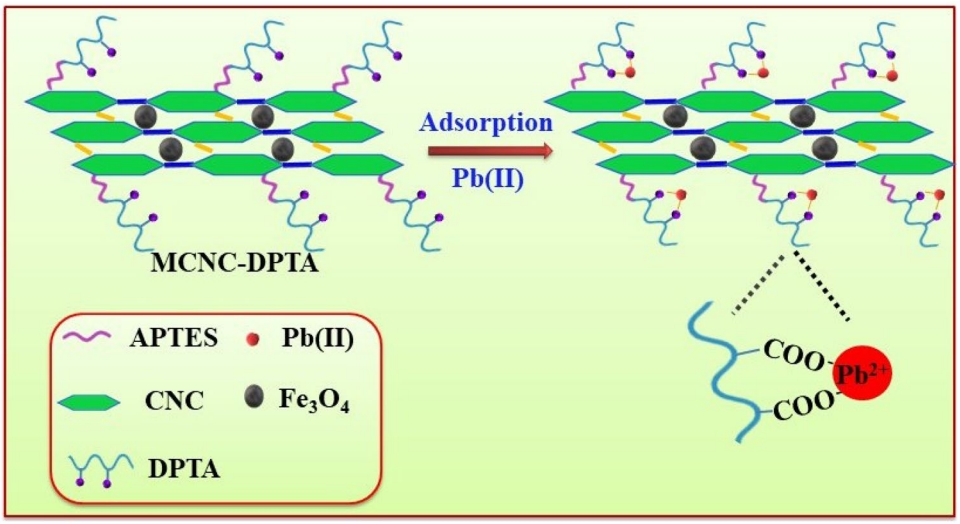

Fig. 1 Mechanism diagram of MCNC-DPTA adsorbing Pb(II)

were purchased from Aladdin Chemical Reagent Co., Ltd. (Shanghai, China).

Preparation of MCNC-DPTA

A previously reported coprecipitation method was used to prepare the MCNCs [31]. More specifically, an aqueous solution of 1.25%wt CNCs (160 mL) was initially prepared. After 30 min of feeding nitrogen, $FeCl_3$ (4.8 g) and $FeCl_2$ (1.8 g) were added. To stabilize the pH of the mixed solution at 9–10, ammonia water was added for adjustment, and stirring was continued for a further 30 min. After this time, a freeze-dryer was used to dry the obtained MCNC product.

The preparation of MCNC-DPTA was described in detail previously [32]. Initially, the prepared MCNC (2 g) were dispersed in DMF (100 mL), and APTES (2 mL) was added into it. The next 2 h were stirred under the protection of N_2 atmosphere. Subsequently, pure water (5 mL) was added to hydrolyze the APTES, and after 3 h, ethanol was used to wash the MCNC-separated by magnet. To graft the DPTA onto the MCNC-APTES, DPTA (2 g), EDC (3.82 g), and NHS (1.15 g) were added into pure water (100 mL) and stirred for 2 h to activate the carboxyl groups of DPTA. Subsequently, MCNC-APTES was dispersed in the above solution with stirring at 45 °C for 12 h. After washing and collection of the resulting product, drying was carried out using a freeze-dryer.

Adsorption and Desorption Experiments

For the adsorption experiment, a portion of the adsorbent (10 mg) was added to a conical flask along with the adsorption solution (10 mL) and shaken using a constant-temperature oscillator at 25 °C and 150 rpm. The concentration of Pb(II) in the mother liquor was 1000 mg/mL, and the concentration of Pb(II) was adjusted between 10 and 800 mg/mL by gradual dilution, while the pH of the Pb(II) solution was adjusted to the desired value between 2 and 6 using 0.1 mol/L solutions of HCl and NaOH. After the adsorption process, the concentration of residual Pb(II) was determined by atomic absorption spectrophotometry. Equations (1) and (2) were used to calculate the adsorption amount (q_t, q_e) at a certain moment and at equilibrium respectively, and Eq. (3) was used to calculate the removal ratio (R) of the adsorbent for Pb(II).

$$q_t = \frac{(C_0 - C_t)V}{m} \tag{1}$$

$$q_e = \frac{(C_0 - C_e)V}{m} \tag{2}$$

$$R\% = [(C_0 - C_e)/C_0] \times 100 \tag{3}$$

where at time t, the concentration of Pb(II) is C_t (mg/L), the amount of adsorbent is m (g), the volume of the Pb(II) solution is V (L), and the initial concentration of Pb(II) and the equilibrium concentration are C_0 (mg/L) and C_e (mg/L), respectively.

Results and Discussion

Characterization

TEM

The microstructures of the obtained materials were examined using TEM. The CNC used herein are not the typical needle- or rod-shaped CNC, but sheet-like CNC, and we

characterized their morphology in a previous study [33]. Figure 2a and d show that the spheroidal nanoparticles of Fe_3O_4 exhibited a state of partial aggregation, and a wide particle size distribution of 3–20 nm was recorded. When the magnetic particles and CNC were compounded by coprecipitation, the irregular-shaped CNC were coated on the surface of Fe_3O_4, and the particle size increased to ~ 40 nm (Fig. 2b and e). The introduction of functional macromolecules was also verified by TEM, because the observation of a film on the particle surfaces corresponded to the aggregation of carboxyl-containing macromolecules via hydrogen bonds.

VSM Analysis

The magnetic analysis results for the MCNC and MCNC-DPTA samples are shown in Fig. 3a. The magnetization of MCNC-DPTA was determined to be 42.76 emu/g, which is slightly weaker than that of the MCNC (i.e. 46.70 emu/g). The above-mentioned TEM results and VSM findings conclusively indicate that the successfully grafted DPTA layer decreased the magnetization of the MCNC. However, this slight decrease did not affect the separation rate of the adsorbent in the solution, with collection by magnetic separation being possible in both cases within 15 s.

XRD Analysis

Figure 3b shows the crystal structure of the magnetic material. A group of clear absorption peaks at $2\theta = 30.2$, 35.5, 43.4, 53.5, 57.2, and 62.7° was observed, which correspond to the (220), (311), (400), (422), (511), and (440) planes, respectively [34, 35]. These results indicate that the prepared nanoparticles are composed of a pure crystalline phase.

TGA

The thermogravimetric analysis (TGA) results are shown in Fig. 3c. Based on these results, the evaporation of residual water in the sample was found to occur between room temperature and 120 ℃, with weight losses of 3.41, 5.55, and 3.36% being recorded for CNC, MCNC, and MCNC-DPTA, respectively. As the temperature continued to rise, the pyranose units in CNC began to degrade, resulting in the weight loss ratio of CNC exceeding 90%. Fe_3O_4 exhibited good thermal stability, and almost no degradation was observed under nitrogen protection. Therefore, MCNC was more stable than CNC, and the total proportion is about 44.1%. According to the weight loss rate of MCNC, it could be inferred that the ratio of CNC to Fe in MCNC was ~ 0.8:1. When APTES and DPTA were combined with MCNC, the degradation rate of MCNC-DPTA increased by 7.69%

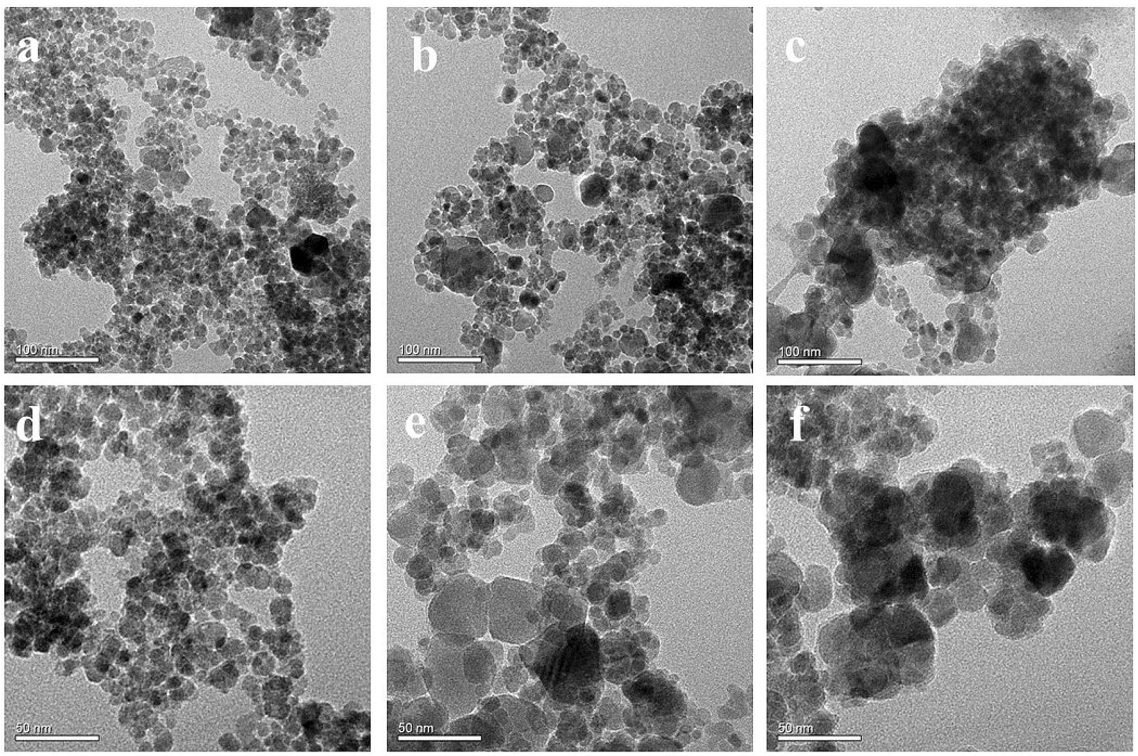

Fig. 2 TEM images at different magnifications: **a**, **d** Fe_3O_4, **b**, **e** MCNC, and **c**, **f** MCNC-DPTA

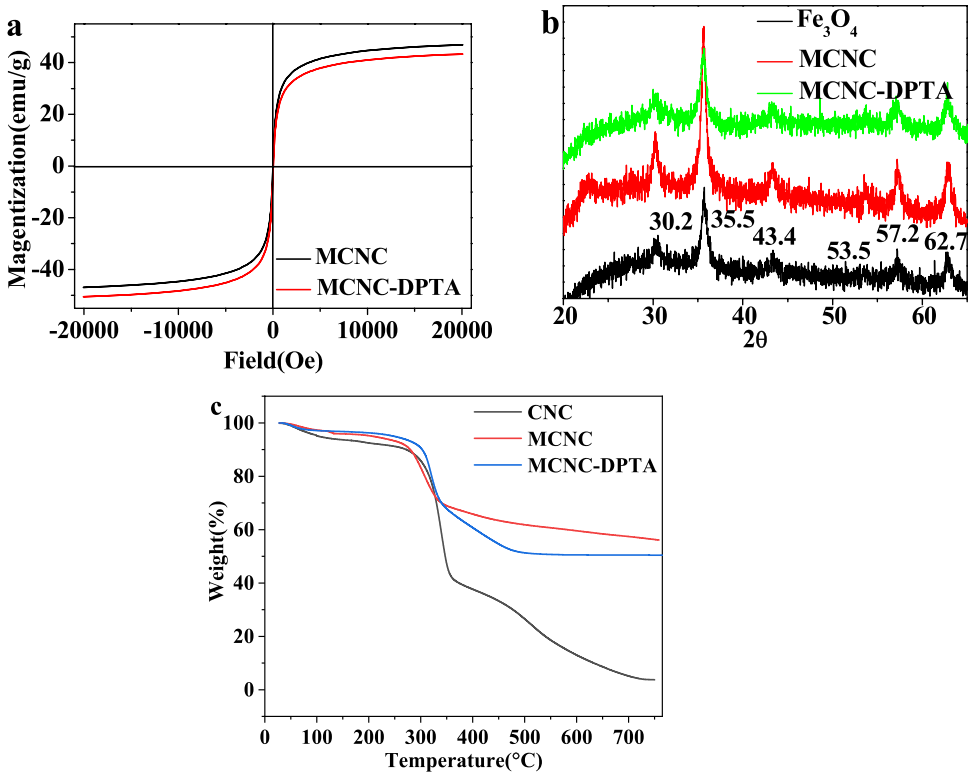

Fig. 3 **a** VSM analysis results of the MCNC and MCNC-DPTA samples; **b** XRD patterns of Fe_3O_4, MCNC, and MCNC-DPTA. **c** TGA curves of CNC, MCNC, and MCNC-DPTA

compared with that of MCNC over the temperature range of 120–550 ℃, which was attributed to the degradation of APTES and DPTA over this temperature range.

FTIR

Figure 4 shows the infrared spectra of the various samples, which indicate the vibration frequency of each functional group in the adsorbent. More specifically, the stretching vibrations of the -OH and Fe–O bonds were located at 3411 and 581 cm^{-1}, respectively [36]. Following CNC grafting onto the surface of Fe_3O_4, the maximum absorption wavelength corresponding to the Fe–O bond shifted from 581 to 621 cm^{-1} because the CNCs have a low dielectric constant, thereby resulting in a dielectric confinement effect. In addition, following the modification of the MCNCs by APTES and DPTA, the characteristic peak of Si–O-C (1034 cm^{-1}) was observed [30, 37], while the stretching vibration of the primary amine group gave only a weak peak at 1338 cm^{-1}, confirming the successful grafting of APTES onto MCNC (Figs. 4b and c) [38]. The observation of the absorption peak corresponding to the primary amide stretching vibration at 1431 cm^{-1} confirmed the successful cross-linking, and the signal at 1649 cm^{-1} indicates the presence of carboxyl groups in the resulting product. Furthermore, the vibration peak at 3270 cm^{1} corresponding to – OH in carboxylic acid, again confirming the successful grafting of DPTA [25].

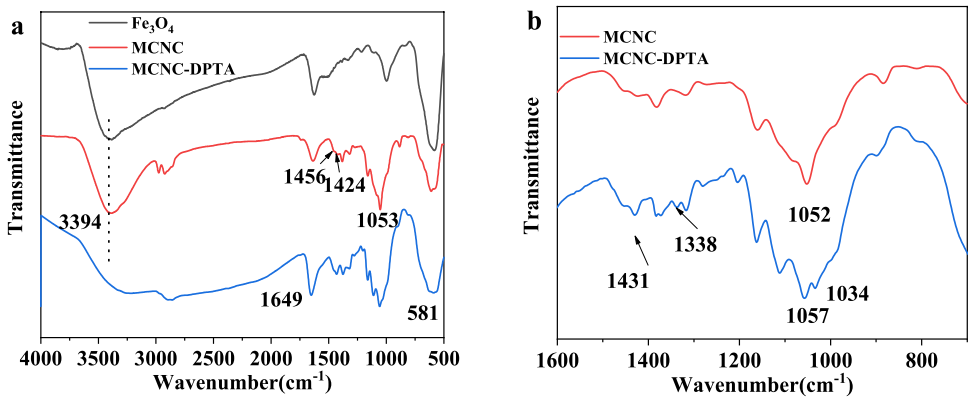

Fig. 4 FTIR spectra of **a** Fe_3O_4, MCNC, and MCNC-DPTA (4000–500 cm^{-1}); and **b** MCNC and MCNC-DPTA (1600–600 cm^{-1})

XPS

The elemental compositions and structures of the MCNC-DPTA and Pb(II)-loaded MCNC-DPTA were then analyzed by XPS. Figure 5a shows a wide scan of the MCNC-DPTA, wherein the Si2p peak originates from APTES, the Fe2p signal belongs to Fe_3O_4, and a clear signal appears at ~ 140 eV (Fig. 5b) corresponding to Pb4f after the adsorption of Pb(II). Figures 4c and d show the C1s spectra of MCNC-DPTA and the Pb(II)-loaded MCNC-DPTA, wherein the peaks at 287.92 and 286.62 eV are O = C–O and C–O, while the peaks at 286.32 and 284.77 eV are O = C–N and C–C [39]. Among them, the O–C = O peak was considered DPTA, confirming that DPTA was successfully grafted onto the MCNCs. In addition, the O = C–N peak originated from the reaction of the amino groups of APTES with the carboxyl groups of DPTA. After the completion of the Pb(II) adsorption process, the positions of these four peaks moved to 287.97, 286.32, 286.72, and 284.62 eV due to coordination between the carboxyl and hydroxyl groups and the heavy metal ions. The changes in the position of the O1s signals before and after adsorption (Figs. 5e and f) confirm that adsorption took place. In this case, both peaks corresponding to O–C = O and C = O originate from DPTA [40], whereas the peak assigned to C–O originates from the CNCs. Following the adsorption of Pb(II), these three peaks moved from 532.62, 532.62, and 530.37 eV to 532.67, 532.27, and 530.27 eV, respectively, indicating that the carboxyl group is involved in the adsorption process.

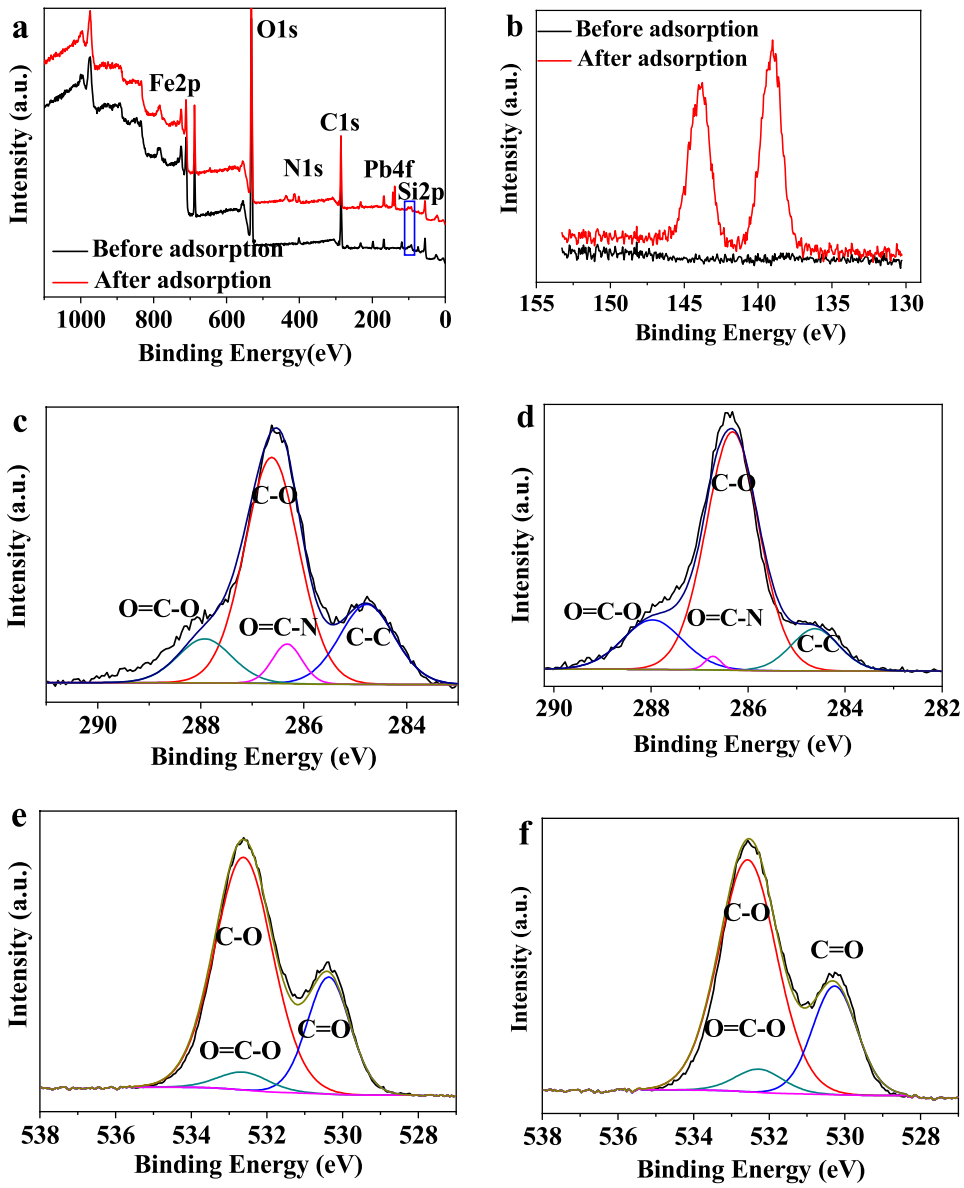

Fig. 5 XPS profiles of MCNC-DPTA and MCNC-DPTA after the loading of Pb(II): **a** wide spectra, **b** Pb4f spectra, **c**, **d** C1s spectra, **e**, **f** O1s spectra before and after adsorption

Factors Affecting the Adsorption Capacity

To a great extent, pH is known to affect the adsorption capacity because it can change the protonation state of the functional groups of an adsorbent. Since Pb(II) is easily precipitated at pH > 6, we examined the adsorption capacities of our adsorbents between pH 2 and 6. As can be seen in Fig. 6a, the adsorption amount increased in a linear manner between pH 2 and 5; thereafter, the adsorption amount did not increase very steeply. Note that each DPTA molecule contains five carboxyl groups, which have pKa values of 1.94, 2.87, 4.37, 8.69, and 10.56; therefore, the number of deprotonated carboxyl groups (i.e., 3) does not change between pH 5 and 6, resulting in similar adsorption capacities (i.e., 187.48 and 190.85 mg/g, respectively). When the concentration of Pb(II) solution was 200 mg/L (pH = 5.56), which affords a corresponding adsorption capacity of 189.72 mg/g, we decided not to artificially adjust the pH value of the solution.

In order to further explain the relationship between the heavy-metal-ion concentration and the adsorption equilibrium time, three Pb(II) concentrations were employed, namely, 100, 200, and 300 mg/L (Fig. 6b). More specifically, these solutions afforded adsorption capacities of 97.96, 189.72, and 272.34 mg/g, corresponding to equilibrium times of 90, 110, and 130 min. This increase in the adsorption rate at higher adsorbate concentrations can be attributed to the fact that higher concentrations of Pb(II) produce greater numbers of interactions with the adsorption sites present on MCNC-DPTA.

Furthermore, the effects of the adsorption temperature and the adsorbate concentration on the adsorption capacity were investigated; the results are presented in Fig. 6c. For these experiments, Pb(II) concentrations of 10–800 mg/L were heated at 293, 298, and 303 K. When the concentration of Pb(II) was between 10 mg/L and 300 mg/L, the adsorption amount of Pb(II) on MCNC-DPTA increased rapidly, with slower increases at concentrations above 300 mg/L, indicating that the adsorption process had reached equilibrium. In addition, increasing the temperature promoted the adsorption process, but only when adsorbate concentrations of > 300 mg/L were employed. In this case, the increase in adsorption performance was attributed to higher temperatures accelerating the movement (i.e., Brownian motion) of the ions in solution, thereby increasing the probability of contact between Pb(II) and the adsorbent.

Moreover, the reusability of an adsorbent is a key factor in determining its applicability and economic value. Thus, we employed a readily available dilute HCl solution to desorb Pb(II) from the MCNC-DPTA. As shown in Fig. 6d, after 6 reuse cycles, the adsorption capacity decreased by only 7%, indicating that this adsorbent continues to exhibit good stability after acid treatment.

Pb(II) Adsorption Kinetics Fitting

The adsorption kinetics model based on chemical adsorption and physical adsorption was therefore established by fitting the adsorption time and the adsorption amount. More

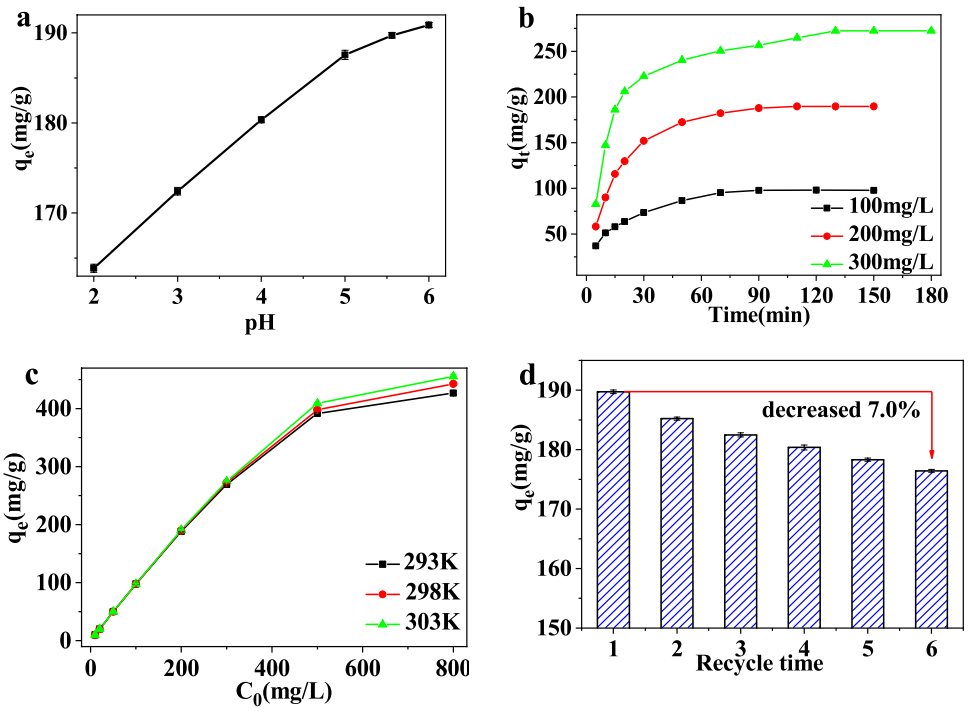

Fig. 6 Effects of various factors on adsorption capacity: **a** pH, **b** adsorption time, **c** initial Pb(II) concentration, and **d** recycle time

specifically, the pseudo first- and second-order formulae can be written as follows:

$$\ln(q_e - q_t) = \ln q_e - k_1 t \tag{4}$$

$$\frac{t}{q_t} = \frac{1}{k_2 q_e^2} + \frac{t}{q_e} \tag{5}$$

where k_1 and k_2 are the model constants. The equilibrium adsorption capacity (q_e) could be obtained from the fitting parameter [40].

The first order kinetic model mainly corresponds to surface adsorption, while the second order kinetic model tends to relate to a chemical adsorption process. The fitted results for our experiments are presented in Fig. 7, and other related parameters are provided in Table 1. As can be seen from these results, the second-order model is a better fit to the adsorption process (i.e., 0.978 (100 mg/L), 0.995 (200 mg/L), and 0.984 (300 mg/L)) than the pseudo-first order model (i.e., 0.926 (100 mg/L), 0.989 (200 mg/L), and 0.971 (300 mg/L)), thereby indicating that the adsorption of Pb(II) by MCNC-DPTA is dominated by chemical adsorption. Moreover, k_2 decreases inversely with the initial concentration, and the adsorption process is promoted at higher initial concentrations.

Pb(II) Adsorption Isotherm Fitting

Two models were then introduced to further interpret the adsorption isotherms, and the nonlinear equations for these models are as follows.

$$\text{Freundlich isotherm model}: q_e = K_F C_e^n \tag{6}$$

$$\text{Langmuir isotherm model}: q_e = \frac{q_m K_L C_e}{1 + K_L C_e} \tag{7}$$

where K_F is the Freundlich adsorption constant affecting the adsorption amount, n is the adsorption constant affecting the adsorption intensity, K_L is the adsorption constant of the Langmuir model, and q_m is the maximum adsorption amount; their values can be calculated from the fitting results. In particular, the Langmuir isotherm model considers a monolayer adsorption process, assuming chemisorption as the premise. On the other hand, as an empirical equation, the Freundlich isotherm model has additional conditions, and considers a non-uniform sorption of multiple layers [41]. The nonlinear fitting curves and relevant data for the adsorption process of MCNC-DPTA at 293.3, 298.3, and 303.3 K are shown in Fig. 8 and Table 2. Due to the fact that higher fitting coefficients (i.e., 0.971, 0.973, and 0.971) were obtained for the Langmuir isotherm model, this model was considered to better describe the adsorption process. Furthermore, upon increasing the adsorption temperature, q_m showed an increasing trend and the binding constant (K_L) also increased, confirming that the adsorption process progressed more smoothly with the increase of adsorption temperature. According to the Freundlich model, the adsorption amount index, 1/n, is between 0 and 1, indicating the adsorption is availed. Moreover, for Pb(II), the q_m values of MCNC-DPTA at 293.3, 298.3, and 303.3 K were determined to be 424.78, 424.67, and 440.0 mg/g, respectively. A comparison of the q_m value of MCNC-DPTA with

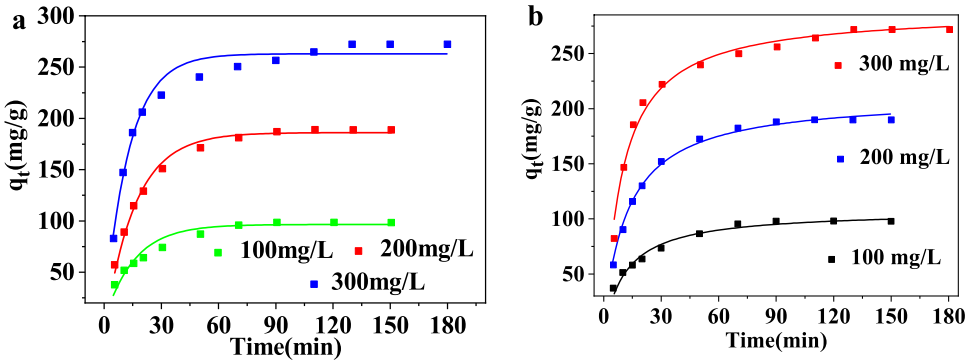

Fig. 7 Plots of adsorption kinetic models: **a** pseudo-first and **b** pseudo-second kinetic order models

Table 1 Kinetic parameters for the adsorption of Pb(II) on MCNC-DPTA

Concentration (mg/L)	Pseudo-first order			Pseudo-second order		
	Δq (mg/g)	k_1 (min^{-1})	R^2	Δq (mg/g)	k_2 (g mg^{-1} min^{-1})	R^2
100	2.62	0.063	0.926	−9.52	7.87×10^{-4}	0.978
200	2.90	0.062	0.984	−21.52	3.77×10^{-4}	0.995
300	10.57	0.077	0.972	−16.50	3.64×10^{-4}	0.984

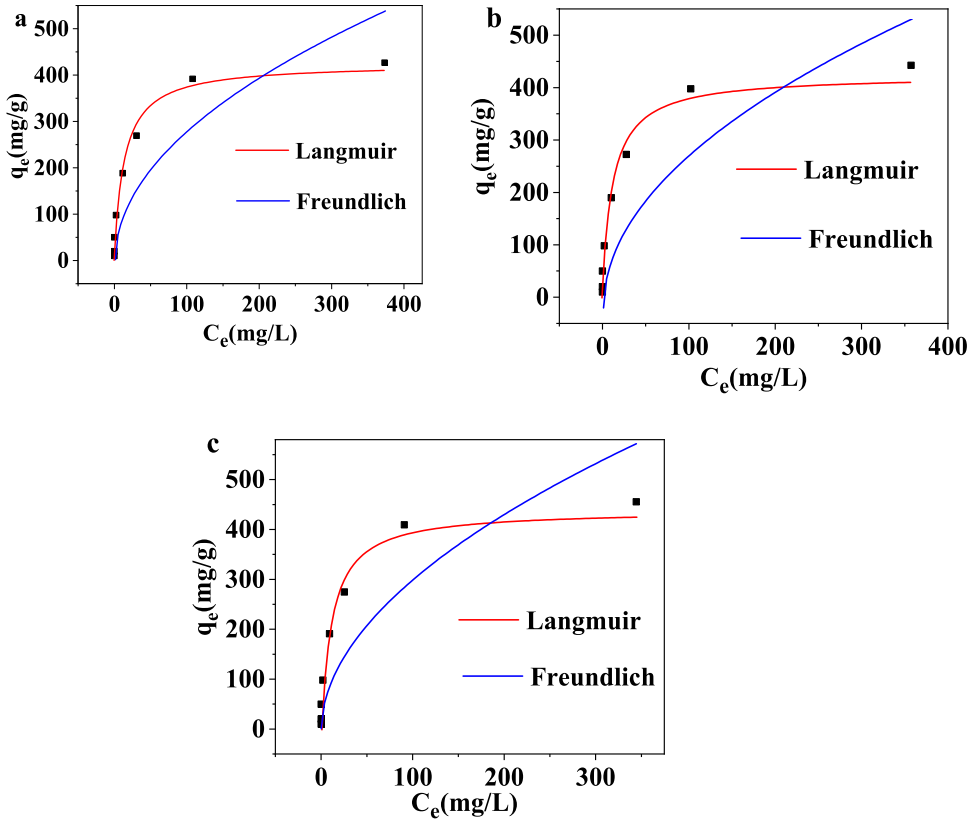

Fig. 8 A Isothermal adsorption models of MCNC-DPTA for Pb(II) at **a** 293.3 K, **b** 298.3 K, and **c** 303.3 K

Table 2 Langmuir and Freundlich isotherm parameters for the adsorption of Pb(II) by MCNC-DPTA

Temperature (K)	Langmuir			Freundlich		
	q_m (mg/g)	K_L (L/min)	R^2	K_F (mg/g)	n ($g \cdot mg^{-1} \cdot min^{-1}$)	R^2
293.3	424.78	0.073	0.971	27.77	2.0	0.73
298.3	424.67	0.084	0.973	29.16	2.0	0.74
303.3	440.0	0.087	0.971	26.37	1.9	0.70

Table 3 Pb(II) adsorption capacities of MCNC-DPTA and previously reported adsorbents

Adsorbent	q_m (mg/g)	Ref.
[a]CS/NFC aerogel	252.6	[42]
[b]CMC-NMO	290.8	[43]
[c]SINC	85	[44]
[d]RH_{MW}-X	295.20	[45]
[e]MCCN	72.83	[46]
MCNC-DPTA	424.67	This work

[a]*CS/NFC aerogel* Chitosan/nano fibrillated cellulose aerogel, [b]*CMC-NMO* cellulose microcrystalline-manganese dioxide nanocomposite, [c]*SINC* sodium itaconate grafted nanocellulose, [d]RH_{MW}-*X* microwave-functionalized cellulose, [e]*MCCN* Magnetic carboxylated cellulose nanocrystals

reported Pb(II) adsorbents (Table 3) apparently indicated that MCNC-DPTA exhibited a higher adsorption performance. Our results therefore indicate that the grafting of DPTA onto MCNC results in a significant improvement in the adsorption capacity toward Pb(II).

Conclusion

We herein reported the preparation of a novel adsorbent, namely DPTA-modified magnetic cellulose nanocrystals (MCNC-DPTA). Investigation of the adsorption behavior of this material indicated that the natural initial pH of the aqueous Pb(II) solution was optimal for the adsorption process, and higher temperatures were found to facilitate adsorption, with maximum Pb(II) adsorption capacities of 424.78, 424.67, and 440.0 mg/g being obtained at 293.3, 298.3, and 303.3 K, respectively. In addition, upon increasing the

initial Pb(II) concentration, a longer adsorption time was required to reach equilibrium. A study into the adsorption kinetic and isotherm models showed that the adsorption process is dominated by chemical adsorption on a uniform surface. Overall, our results indicated that the satisfactory recycling performance and adsorption capacity of the prepared MCNC-DPTA render it an excellent material for the removal of Pb(II). These results are of importance because the development of mild methods for cellulose modification is required to improve the applicability and effectiveness of CNC-based materials as a heavy metal adsorbent.

Acknowledgements This work was supported by the and the National Natural Science Foundation of China (21606136, 21476212), Zhejiang Provincial Key Laboratory of Health Risk Appraisal for Trace Toxic Chemicals (2021001, 2021002).

Author Contributions JS: Investigation, Funding acquisition. FJ Investigation and Data curation. NW: writing-Original Draft. XO: Conceptualization, Methodology, Funding acquisition. MJ: Supervision, Funding acquisition.

Declarations

Conflict of Interest The authors declare that they have no conflict of interest.

References

1. He Y, Tian H, Xiang A, Wang H, Li J, Luo X, Rajulu AV (2021) Fabrication of PVA nanofibers grafted with octaamino-POSS and their application in heavy metal adsorption. J Polym Environ 29(5):1566–1575
2. S.M. Wong, M.Z.A. Zulkifli, D. Nordin, Y.H. Teow, Synthesis of cellulose/nano-hydroxyapatite composite hydrogel absorbent for removal of heavy metal ions from palm oil mill effluents, Journal of Polymers and the Environment (2021).
3. Elsherbiny AS, El-Hefnawy ME, Gemeay AH (2018) Adsorption efficiency of polyaspartate-montmorillonite composite towards the removal of Pb(II) and Cd(II) from aqueous solution. J Polym Environ 26(2):411–422
4. Li C, Ma H, Venkateswaran S, Hsiao BS (2020) Highly efficient and sustainable carboxylated cellulose filters for removal of cationic dyes/heavy metals ions. Chem Eng J 389:123458
5. Lian Q, Ahmad ZU, Gang DD, Zappi ME, Fortela DLB, Hernandez R (2020) The effects of carbon disulfide driven functionalization on graphene oxide for enhanced Pb(II) adsorption: Investigation of adsorption mechanism. Chemosphere 248:126078–126078
6. Betiha MA, Moustafa YM, Mansour AS, Rafik E, El-Shahat MF (2020) Nontoxic polyvinylpyrrolidone-propylmethacrylate-silica nanocomposite for efficient adsorption of lead, copper, and nickel cations from contaminated wastewater. J Mol Liq 314:113656
7. Duan Y, Tan J, Huang Z, Deng Q, Liu S, Wang G, Li L, Zhou L (2020) Facile synthesis of carboxymethyl cellulose sulfur quantum dots for live cell imaging and sensitive detection of Cr(VI) and ascorbic acid. Carbohydrate Poly 249:116882
8. D. Hu, H. huang, R. Jiang, N. Wang, H. Xu, Y. G. Wang, X. K. Ouyang, Adsorption of diclofenac sodium on bilayer amino-functionalized cellulose nanocrystals/chitosan composite. J. Hazard. Mater. 369 (2019) 483–493.
9. A. Pal, T. Das, S. Sengupta, S. Sardar, S. Mondal, A. Bandyopadhyay, An elastic semi IPN polymer hybrid for enhanced adsorption of heavy metals, Carbohyd. Polym. 236 (2020).
10. He W, Yu Q, Wang N, Ouyang X-K (2020) Efficient adsorption of Cu(II) from aqueous solutions by acid-resistant and recyclable ethylenediamine tetraacetic acid-grafted polyvinyl alcohol/chitosan beads. J Mol Liq 316:113856
11. E. Cerrahoğlu Kaçakgil, S. Çetintaş, Preparation and characterization of a novel functionalized agricultural waste-based adsorbent for Cu2+ removal: Evaluation of adsorption performance using response surface methodology, Sustainable Chemistry and Pharmacy 22 (2021) 100468.
12. Kayan GO, Kayan A (2021) Composite of natural polymers and their adsorbent properties on the dyes and heavy metal ions. J Polym Environ. https://doi.org/10.1007/s10924-021-02154-x
13. Gao P, Lei J, Tan J, Wang G, Liu H, Zhou L (2021) Self-assembled magnetic microcrystalline cellulose/MoS2/Fe_3O_4 composite for efficient adsorptive removal of mercury ions (Hg^{2+}). Comp Commun 25:100736
14. T. Zhang, Y. Zhao, M.S. Silverstein, Cellulose-based, highly porous polyurethanes templated within non-aqueous high internal phase emulsions, Cellulose (2020) 4007–4018.
15. Naghdi T, Golmohammadi H, Yousefi H, Hosseinifard M, Kostiv U, Horak D, Merkoci A (2020) Chitin nanofiber paper toward optical (Bio)sensing applications. ACS Appl Mater Interfaces 12(13):15538–15552
16. Yang Y, Xie B, Liu Q, Kong B, Wang H (2020) Fabrication and characterization of a novel polysaccharide based composite nanofiber films with tunable physical properties. Carbohyd Polym 236:116054
17. Khodayari A, Van Vuure AW, Hirn U, Seveno D (2020) Tensile behaviour of dislocated/crystalline cellulose fibrils at the nano scale. Carbohyd Polym 235:115946
18. Ren J, Tao F, Cui Y (2020) L-glutamic acid crosslinked cellulose ester films for heavy metal ions adsorption. J Polym Environ 28(4):1302–1314
19. Debiagi F, Faria-Tischer PCS, Mali S (2020) Nanofibrillated cellulose obtained from soybean hull using simple and eco-friendly processes based on reactive extrusion. Cellulose 27(4):1975–1988
20. Nechyporchuk O, Belgacem MN, Bras J (2016) Production of cellulose nanofibrils: A review of recent advances. Ind Crops Prod 93:2–25
21. Ogunsona EO, Panchal P, Mekonnen TH (2019) Surface grafting of acrylonitrile butadiene rubber onto cellulose nanocrystals for nanocomposite applications. Compos Sci Technol 184:10
22. Esmaeilzade B, Esmaielzadeh S, Ahmadizadegan H (2018) Ultrasonic irradiation to modify the functionalized bionanocomposite in sulfonated polybenzimidazole membrane for fuel cells applications and antibacterial activity. Ultrason Sonochem 42:260–270
23. Ren Y, Abbood HA, He F, Peng H, Huang K (2013) Magnetic EDTA-modified chitosan/SiO2/Fe3O4 adsorbent: Preparation, characterization, and application in heavy metal adsorption. Chem Eng J 226:300–311
24. Chen B, Zhao H, Chen S, Long F, Huang B, Yang B, Pan X (2019) A magnetically recyclable chitosan composite adsorbent functionalized with EDTA for simultaneous capture of anionic dye and heavy metals in complex wastewater. Chem Eng J 356:69–80
25. Li B, Li M, Zhang J, Pan Y, Huang Z, Xiao H (2019) Adsorption of Hg (II) ions from aqueous solution by diethylenetriaminepentaacetic acid-modified cellulose. Int J Biol Macromol 122:149–156
26. Ding C, Sun L, Xiao G, Qian X, An X (2017) Green and combinational method towards clickable alkynylated cellulose fibers (ACFs). Cellulose 24(8):3219–3229

27. D.J. Mendoza, C. Browne, V.S. Raghuwanshi, G.P. Simon, G. Garnier, One-shot TEMPO-periodate oxidation of native cellulose, Carbohyd. Polym. 226 (2019).
28. Gun'ko VM, Voronin EF, Pakhlov EM, Zarko VI, Turov VV, Guzenko NV, Leboda R, Chibowski E (2000) Features of fumed silica coverage with silanes having three or two groups reacting with the surface. Colloids Surf A 166(1–3):187–201
29. Khoobi M, Delshad TM, Vosooghi M, Alipour M, Hamadi H, Alipour E, Hamedani MP, Ebrahimi SES, Safaei Z, Foroumadi A, Shafiee A (2015) Polyethyleneimine-modified superparamagnetic Fe3O4 nanoparticles: An efficient, reusable and water tolerance nanocatalyst. J Magn Magn Mater 375:217–226
30. Kayan GO, Kayan A (2021) Inorganic-organic hybrid materials of zirconium and aluminum and their usage in the removal of methylene blue. J Inorg Organomet Polym Mater 31(8):3613–3623
31. Wang Y-F, Wang Y-G, Ouyang X-K, Yang L-Y (2017) Surface-imprinted magnetic carboxylated cellulose nanocrystals for the highly selective extraction of six fluoroquinolones from egg samples. ACS Appl Mater Interfaces 9(2):1759–1769
32. Jouyandeh M, Jazani OM, Navarchian AH, Shabanian M, Vahabi H, Saeb MR (2018) Surface engineering of nanoparticles with macromolecules for epoxy curing: Development of super-reactive nitrogen-rich nanosilica through surface chemistry manipulation. Appl Surf Sci 447:152–164
33. Wang N, Ouyang X-K, Yang L-Y, Omer AM (2017) Fabrication of a magnetic cellulose nanocrystal/metal–organic framework composite for removal of Pb(II) from water. ACS Sustainable Chemistry & Engineering 5(11):10447–10458
34. Foong LK, Khojasteh H, Amiri M, Heydaryan K, Salavati-Niasari M, Almasi-Kashi M, Lyu ZJ (2020) Environmental friendly approach for facile synthesis of graphene-like nanosheets for photocatalytic activity. J Alloy Compd 823:10
35. Huang B, Lu M, Wang D, Song Y, Zhou L (2018) Versatile magnetic gel from peach gum polysaccharide for efficient adsorption of Pb^{2+} and Cd^{2+} ions and catalysis. Carbohyd Polym 181:785–792
36. Jia Y, Wang Y, Yan M, Wang Q, Xu H, Wang X, Zhou H, Hao Y, Wang M (2020) Fabrication of iron oxide@MOF-808 as a sorbent for magnetic solid phase extraction of benzoylurea insecticides in tea beverages and juice samples. J Chromatogr A 1615:460766–460766
37. Wang W, Wen T, Bai H, Zhao Y, Ni J, Yang L, Xia L, Song S (2020) Adsorption toward Cu(II) and inhibitory effect on bacterial growth occurring on molybdenum disulfide-montmorillonite hydrogel surface. Chemosphere 248:126025–126025
38. Doaga R, McCormac T, Dempsey E (2020) Functionalized magnetic nanomaterials for electrochemical biosensing of cholesterol and cholesteryl palmitate. Microchim Acta 187(4):10
39. Chen D, Wang XB, Wang XL, Feng K, Su JC, Dong JN (2020) The mechanism of cadmium sorption by sulphur-modified wheat straw biochar and its application cadmium-contaminated soil. Sci Total Environ 714:8
40. Sun QL, Tang M, Hendriksen PV, Chen B (2020) Biotemplated fabrication of a 3D hierarchical structure of magnetic ZnFe2O4/MgAl-LDH for efficient elimination of dye from water. J Alloy Compd 829:12
41. Mashkoor F, Nasar A (2020) Magnetized Tectona grandis sawdust as a novel adsorbent: preparation, characterization, and utilization for the removal of methylene blue from aqueous solution. Cellulose 27(5):2613–2635
42. Li YQ, Guo CF, Shi RH, Zhang H, Gong LZ, Dai LB (2019) Chitosan/nanofibrillated cellulose aerogel with highly oriented microchannel structure for rapid removal of Pb (II) ions from aqueous solution. Carbohyd Polym 223:6
43. Fu BB, Xie FC (2020) Facile in situ synthesis of cellulose microcrystalline-manganese dioxide nanocomposite for effective removal of Pb(II) and Cd(II) from water. Environ Sci Pollut Res 27(5):5108–5121
44. Vadakkekara GJ, Thomas S, Nair CPR (2020) Sodium itaconate grafted nanocellulose for facile elimination of lead ion from water. Cellulose 27(6):3233–3248
45. J. Qu, X. Tian, Z. Jiang, B. Cao, M.S. Akindolie, Q. Hu, C. Feng, Y. Feng, X. Meng, Y. Zhang, Multi -component adsorption of Pb(II), Cd(II) and Ni(II) onto microwave-functionalized cellulose: Kinetics, isotherms, thermodynamics, mechanisms and application for electroplating wastewater purification, J. Hazard. Mater. 387 (2020).
46. Lu J, Jin R-N, Liu C, Wang Y-F, Ouyang X-K (2016) Magnetic carboxylated cellulose nanocrystals as adsorbent for the removal of Pb(II) from aqueous solution. Int J Biol Macromol 93:547–556